Applied Catalysis B: Environmental 233 (2018) 1–10

Contents lists available at ScienceDirect

Applied Catalysis B: Environmental

journal homepage: www.elsevier.com/locate/apcatb

# Photocatalytic organic transformations: Simultaneous oxidation of aromatic alcohols and reduction of nitroarenes on $CdLa_2S_4$ in one reaction system

Sujuan Zhang[a,b], Weixin Huang[a,*], Xianliang Fu[b,*], Xiuzhen Zheng[b], Sugang Meng[b], Xiangju Ye[c], Shifu Chen[b,c,**]

[a] Hefei National Laboratory for Physical Sciences at the Microscale, CAS Key Laboratory of Materials for Energy Conversion, Department of Chemical Physics, University of Science and Technology of China, Hefei, 230026, Anhui, China
[b] College of Chemistry and Material Science, Huaibei Normal University, Huaibei, 235000, Anhui, China
[c] Department of Chemistry, Anhui Science and Technology University, Fengyang, 233100, Anhui, China

ARTICLE INFO

*Keywords:*
$CdLa_2S_4$
Selective organic transformation
Aromatic alcohols
Nnitroarenes
Photocatalytic

ABSTRACT

Photocatalytic selective organic transformations (SOTs) with sunlight offer a "green" route for synthesis of fine chemicals. In this work, a bare ternary chalcogenide $CdLa_2S_4$ photocatalyst was fabricated to couple the selective oxidation (SO) of aromatic alcohols to aldehydes and selective reduction (SR) of nitroarenes to anilines in one reaction system. The photocatalyst showed a high stability and a good generality for the conversions due to the well–matched band structure and the high separation efficiency of photoinduced electrons (e–) and holes ($h^+$). For p–substituted aromatic alcohols, the selectivities to the corresponding aldehydes are as high as *ca.* 90%. The electro–donating substituent in the para position benefits the SO reactions, which are triggered by $h^+$ via a successive deprotonation; while for p–substituted nitroarenes, the SR to the corresponding anilines is vulnerable to the electro–withdrawing groups and the steric hindrance of the substituent and the selectivities to anilines are substantially lower than that of the SO conversions. $H^+$ deprotonated in the SO of aromatic alcohols is indispensable for the SR of nitroarenes as they are achieved by a $H^+$–coupled six e– reduction process, which leads to the low conversion efficiencies. The half conversions not only be coupled by the photoinduced e– and $h^+$, but also collaborate with each other through $H^+$. Our results clearly demonstrate the emerging concept of a coupled reaction system for sunlight–driven synthesis of fine chemicals and reveal the underlying mechanism.

## 1. Introduction

Due to their mild and "green" reaction conditions, selectively organic transformations (SOTs) on heterogeneous photocatalyst have drawn extensive attention for solar chemicals in recent years [1–5]. As the photoinduced electron (e–) and hole ($h^+$) have a reduction and oxidation capability, respectively, the transformations of organics on activated semiconductor photocatalyst mainly focus on redox conversions. Photocatalytic selective oxidation (SO) of aromatic alcohols into the corresponding aromatic aldehydes [6–12] and selective reduction (SR) of nitroarenes to the corresponding amino organics [13–19] are the most two well–known reactions as the products are important organic compounds or intermediates for the synthesis of pharmaceuticals, fragrance, and other fine chemicals.

The traditional SO of alcohols was mainly carried out by a non-catalytic process with use of stoichiometric environmentally unfriendly oxidants such as potassium permanganate, chromic acid, and potassium dichromate, which not only produces a large amount of toxic and hazardous waste, but also involves a separation issue of the products. To overcome these defects, tremendous efforts have been devoted to develop new catalytic systems with $O_2$ as the oxidant. For this end, some noble metal supported oxides have been developed as the SO catalyst [20–22]. However, the conversion still limited by the cost of the catalyst, as well as the harsh reaction conditions of high temperature or high pressure. Whereas for SR of nitro compounds, it is commercially reduced with Sn/Fe-HCl or high pressure $H_2$ catalysed by precious metal catalysts [23–26], which results in a waste-disposal problem or safety issues. Therefore, it is still an important research subject to develop a highly selective, safe and environmentally benign process for both the SO and SR conversions. One encouraging approach is to perform these conversions by a photocatalytic process at room temperature with sunlight as a driving force and $O_2$ and alcohols as oxidant and safety hydrogen source, respectively. Many efforts have been devoted to this area in recent years and dye–sensitized $TiO_2$ [6], g–$C_3N_4$ [27,28],

* Corresponding authors.
** Corresponding author at: College of Chemistry and Material Science, Huaibei Normal University, Huaibei, 235000, Anhui, China.
*E-mail addresses:* huangwx@ustc.edu.cn (W. Huang), fuxiliang@gmail.com (X. Fu), chshifu@chnu.edu.cn (S. Chen).

https://doi.org/10.1016/j.apcatb.2018.03.084
Received 28 January 2018; Received in revised form 3 March 2018; Accepted 24 March 2018
Available online 26 March 2018
0926-3373/ 

$Bi_{12}O_{17}Cl_2$ [12], BiOCl [11], and some chalcogenides [17,29–34] have been used as the photocatalyst. To further enhance the conversion efficiencies, some graphene modified $TiO_2$, chalcogenides and BN–based semiconductor composites photocatalysts were further developed [30,35–38], which can facilitate the separation of photoinduced charge carriers or extend the utilization of visible light, respectively. Although some important progresses have been made, [6,7,11,16–18] efforts from the perspectives of the photocatalyst and the reaction system are still required to further improve the conversion efficiency.

As the objective of SOTs is to oxidize or reduce the organics to the desired intermediates rather than to the mineralization products like $H_2O$ and $CO_2$, a semiconductor with a mild band-gap energy is more promising than wide-band-gap sample. Binary and ternary chalcogenides, such as CdS, $In_2S_3$, $ZnIn_2S_4$, and $CdIn_2S_4$, are typical narrow–band-gap semiconductors and are promising candidates for SOTs under visible light irradiation [32–34,39]. Recently, we found that the SO of aromatic alcohol to the corresponding aldehyde can be achieved on $ZnIn_2S_4$ and CdS photocatalysts [33,39]. Unfortunately, CdS holds the drawback of photocorrosion during irradiation, which leads to a deactivation of CdS during the reactions. Therefore, developing a high efficiency and stable photocatalyst for SOTs is still required.

Another strategy to improve the SOTs efficiency is to optimize the photocatalytic reaction system. At present, most of the reaction systems are concentrated only on the semi–conversion, *i.e.* SO or SR reaction [7,11,16,40,41]. It means that only e– or $h^+$ is involved in the conversion of organics, while the opponent is consumed by scavengers and not involved in SOTs. $O_2$, $AgNO_3$, and $(NH_4)_2S_2O_8$ were commonly used as e– acceptors for SO conversions [8,11,28,42,43], while $CH_3OH$, $HCOONH_4$, $(NH_4)_2C_2O_4$, HCOOH, and hydrazine hydrate were used as $h^+$ scavengers for SR conversions [16,18,28,44–46]. From the perspective of the reaction model, the SO and SR of organics can be coupled into one reaction system if the semi–conversions can coordinate with each other. The quantum efficiency of SOTs then can be doubled. The feasibility of this kind of reaction system is determined by the nature of the conversions and the band structure of the photocatalyst, which can match well with the conversions. Unfortunately, this type of conversion system is still rare. Recently, we found that the SO of aromatic alcohols by photogenerated $h^+$ and SR of nitroarenes by e– could be coupled in one reaction system on CdS and $CdIn_2S_4$ [34,39]. These works suggest that the coupling system for SOTs is feasible. But a highly efficient and stable photocatalyst is still required and the synergistic mechanism between the SO and SR conversions needs to be further elucidated.

As a ternary semiconductor chalcogenide, $CdLa_2S_4$ has a suitable band gap *ca.* 2.4 eV [47–49] corresponding well with visible light absorption. Previous works [47,48] revealed that $CdLa_2S_4$ was active for photocatalytic degradation of organic pollutants and splitting of water for hydrogen evolution under visible light irradiations. Considering that $CdLa_2S_4$ has a similar component and structure to that of the reported $CdIn_2S_4$, it has a great potential for photocatalytic SOTs as that observed on $CdIn_2S_4$ [34]. However, there is still no report on the use of $CdLa_2S_4$ for SOTs. Based on the above considerations, in this work, we developed a facile solvothermal method to fabricate $CdLa_2S_4$ photocatalyst. SO of aromatic alcohols and SR of nitroarenes in a coupled reaction system over $CdLa_2S_4$ were then investigated under visible light irradiation. The synergistic mechanism between the semi–conversions was finally studied.

## 2. Experimental section

### 2.1. Materials

Cadmium nitrate ($Cd(NO_3)_2{\cdot}4H_2O$, 99%), lanthanum nitrate ($La(NO_3)_3{\cdot}6H_2O$, 99%), thiacetamide ($C_2H_5NS$, TAA, ≥99.0%), ethylenediamine ($C_2H_4(NH_2)_2$, EDA,>99%), benzotrifluoride ($C_6H_5CF_3$, BTF, 99.0%), p–methoxybenzyl alcohol ($C_6H_5OCH_3CH_2OH$, p–MBA, 98.0%), p–methoxybenzaldehyde ($C_6H_5OCH_3CHO$, p–MBAD, 98.0%), nitrobenzene ($C_6H_5NO_2$, NB, 99.0%), nitrosobenzene ($C_6H_5NO$, NSB, 99.0%), aniline ($C_6H_7N$, AL, ≥99.0%), benzyl alcohol ($C_6H_5CH_2OH$, ≥99.0%), benzaldehyde ($C_6H_5CHO$, ≥99.0%), p–chlorobenzyl alcohol ($C_6H_4ClCH_2OH$, ≥99.0%), 4–chlorobenzaldehyde ($C_6H_4ClCHO$, ≥99.0%), p–fluorobenzyl alcohol ($C_6H_4FCH_2OH$, ≥99.0%), 4–fluorobenzaldehyde ($C_6H_4FCHO$, ≥99.0%), 4–Nitrotoluene ($C_7H_7NO_2$, ≥99.0%), 4–chloronitrobenzene ($C_6H_4ClNO_2$, ≥99.5%), 4–fluoronitrobenzene ($C_6H_4FNO_2$, ≥99.0%), triethanolamine ($C_6H_{15}NO_3$, 98.0%), tetrachloromethane ($CCl_4$, 99.5%), lithium perchlorate ($LiClO_4$, 99.9%), potassium ferricyanide ($K_3Fe(CN)_6$, ≥99.5%), potassium ferrocyanide trihydrate ($K_4Fe(CN)_6{\cdot}3H_2O$, 99.0%), potassium chloride (KCl, 99.5%) and sodium sulfate anhydrous ($Na_2SO_4$, 99.0%) were purchased from Aladdin Reagent (Shanghai, China) and used as received.

### 2.2. Preparation of photocatalysts

$CdLa_2S_4$ was prepared by a solvothermal method. 2.5 mmol $Cd(NO_3)_2{\cdot}4H_2O$, 5 mmol $La(NO_3)_3{\cdot}6H_2O$, and 22.5 mmol TAA were first dissolved in 60 mL EDA, followed by stirring for 20 min. The homogeneous solution was then transferred into a 100 mL Teflon–lined stainless steel autoclave and was kept at 180 °C for 24 h. After cooling to room temperature, the precipitates were collected by centrifugation and washed thoroughly with absolute ethanol and deionized water alternately. The final product was dried in a vacuum oven at 60 °C for 8 h.

CdS was used as a reference to compare the activity of $CdLa_2S_4$ and was prepared by a similar solvothermal procedure. 7.5 mmol $Cd(NO_3)_2{\cdot}4H_2O$ and 22.5 mmol TAA were dissolved in 60 mL EDA. After stirring for about 10 min, the mixture solution was transferred into a Teflon–lined stainless autoclave and was then maintained at 180 °C for 24 h. A similar washing and drying procedure was used to collect CdS.

### 2.3. Materials characterization

Powder X–ray diffraction (XRD) patterns were recorded on a Bruker D8 Advance X–ray diffractometer. UV–vis diffuse reflectance spectra (UV–Vis DRS) were determined on a TU-1950 Vis-NIR spectrophotometer (TU-1950, Persee) with $BaSO_4$ as a reference. High–resolution/ Transmission electron microscopy (HR–/TEM) images were collected on a microscope (JEOL, JEM 2100 EX) at an accelerating voltage of 200 kV. The elemental mappings were analyzed by an energy–dispersive X–ray spectrometer (EDS) attached to the SEM instrument (ZEISS SUPRA 40). Photoluminescence (PL) emission spectra were recorded on a JASCO FP–6500 fluorescence spectrophotometer with an excitation wavelength of 440 nm light at room temperature. X–ray photoelectron spectroscopy (XPS) measurement was conducted on a Thermo Scientific ESCA LAB 250 photoelectron spectrometer. All the binding energies were referred to the C 1 s peak of the surface adventitious carbon at 284.6 eV. The Brunauer–Emmett–Teller (BET) of the samples was analyzed by $N_2$ adsorption–desorption on a Micromeritics ASAP 2020.

### 2.4. Photo–electrochemical performance

The charge separation and the transferring resistance of the prepared $CdLa_2S_4$ and CdS were measured by electrochemical impedance spectroscopy (EIS). The experiments were performed on a CHI–660E electrochemical workstation (CHI instruments) in a standard three–electrode cell with the as–prepared samples (5 mm × 5 mm, FTO/$CdLa_2S_4$) as the working electrodes, an Ag/AgCl electrode (in 3 M KCl solution) as the reference electrode, and a Pt wire as the counter electrode, respectively. The thin film working electrodes were prepared by drop–casting samples/$H_2O$ suspensions onto FTO glass substrates followed by drying the film in air overnight. 0.5 M KCl aqueous solution containing $K_3[Fe(CN)_6]$ (0.01 M) and $K_4[Fe(CN)_6]$ (0.01 M) was used as

the electrolyte.

The Mott–Schottky analyses of $CdLa_2S_4$ and CdS were conducted on the same electrochemical workstation system to evaluate the flat band positions ($V_{fb}$) of the prepared $CdLa_2S_4$ and CdS. The potential ranges from –0.3 to 0.2 V (vs Ag/AgCl) at a frequency of 500, 1000, and 1500 Hz. A 0.2 M $Na_2SO_4$ aqueous solution was used as the electrolyte (the pH is *ca.* 7.0) which was purged with $N_2$ before the measurement.

The Cyclic Voltammetry (CV) of the reactants and the productions were measured according to reported procedure[12] to evaluate the redox potentials of p–MBA to p–MBAD and NB to NSB by sweeping at 0.05 V/s. A glass carbon disk, a platinum wire and an Ag/AgCl electrode (3 M) were used as the working, counter, and reference electrodes, respectively. The measurements were performed in acetonitrile in air atmosphere.

### 2.5. Evaluation of photocatalytic activity

Photocatalytic SO of aromatic alcohols to aromatic aldehydes and SR of nitroarenes to anilines were performed in a commercial photochemical reactor (WCGF–100, TaiKang instrument company, Xi'an). A mixture of aromatic alcohol ($2.5 \times 10^{-2}$ mol/L), nitrobenzene ($8.5 \times 10^{-3}$ mol/L), and 0.1 g catalyst were first dispersed in 15 mL BTF. The suspension was then purged with $N_2$ (100 mL/min) for 10 min to remove $O_2$, subsequently the reactor was filled with 0.1 MPa $N_2$. Before turning on the Xe lamp (PLS–SXE 300, $\lambda > 420$ nm), the suspension was stirred in the dark for 30 min to reach an adsorption–desorption equilibrium. The average intensity of the irradiation for the activation of $CdLa_2S_4$ is ca. 1.04 mW $cm^{-2}$ (in the range of 420–520 nm, measured by SpectriLight ILT 950 spectroradiometer) and the irradiation area is ca. 28 $cm^2$. The suspension temperature was controlled at *ca.* 40 °C by a DC–0515 cooling bath (FangRui, Shanghai) during the irradiation. Fig. S1 shows the image of the reaction system. After irradiation for a desired time, the mixture was centrifuged to remove the catalyst particles. The supernatant was then analyzed by a GC (FuLi 9790, China) with a FID detector and a GC–MS technique (Agilent 7890 A-5975C, USA). The Conversion, yield and selectivity for the reactions were calculated by Eqs. (1), (2), and (3), respectively.

$$\text{Conversion (C\%)} = [(C_0–C_r)/C_0] \times 100 \quad (1)$$

$$\text{Yield (Y\%)} = C_p/C_0 \times 100 \quad (2)$$

$$\text{Selectivity (S\%)} = [C_p/(C_0–C_r)] \times 100 \quad (3)$$

where $C_0$ is the initial concentration of the reactants; $C_r$ and $C_p$ are the concentrations of the reactants and the target products after irradiation for a certain time, respectively. For the SR of nitroarenes, besides the final product of aromatic amines, aromatic nitroso compounds, the intermediate reduction products of nitroarenes, were also observed by GC. The yields of the nitroso compounds and the amines are denoted as $Y_1$% and $Y_2$%, respectively.

## 3. Results and discussion

### 3.1. Characterization results

Fig. 1a shows the XRD pattern of the prepared $CdLa_2S_4$. The diffraction peaks can be indexed to cubic phase $CdLa_2S_4$ with a = b = c = 8.7033 Å. [47–49] No peaks originated from CdS or $La_2S_3$ can be perceived suggesting the complete formation of pure phase $CdLa_2S_4$. The three major peaks located at 2θ = 24.4, 30.8, and 43.8° correspond to the (120), (300), (303) planes of cubic $CdLa_2S_4$ and the strong diffraction signals imply the high crystalline nature of the sample. As shown in Fig. 1b, the intrinsic band–gap transition of $CdLa_2S_4$ is threshold at 510 nm, which corresponds to a band–gap energy of 2.39 eV according to the Tauc plot shown in the inset of Fig.1b. Similar band gap energy of $CdLa_2S_4$ has been reported. [47–49] The visible absorption agrees well with the brown color of $CdLa_2S_4$ and offers the potential application of $CdLa_2S_4$ under visible light that accounts for ca. 43% of solar spectrum. Fig. 1c and d show the SEM image of the prepared $CdLa_2S_4$. It shows that the sample is composed of disc–shaped particles with a diameter of *ca.* 500 nm and a thickness of *ca.* 120 nm. The EDS result (Fig. 1e) indicates that the main components of the sample are Cd, La, and S elements and the ratio of Cd:La:S is 1.0:2.1:3.6, which is close to the stoichiometric composition of $CdLa_2S_4$. The morphology feature of $CdLa_2S_4$ was further confirmed by TEM image. The front view image (Fig. 1f) shows that the diameter of the disc particles is *ca.* 450 nm. A careful examination demonstrates that the disc–shaped particles are assembled with a great deal of nano grains. Two sets of lattice fringes with an interplanar spacing of 0.31 and 0.35 nm can be observed in the grains (Fig. 1g), which can be ascribed to the (220) and (121) planes of $CdLa_2S_4$. The angle between the two fringes is measured to be 30° which agrees well with the theoretical interfacial angle (29.9°) between the (220) and (121) plane of cubic $CdLa_2S_4$.

XPS was used to study the surface composition and the chemical states of the elements in $CdLa_2S_4$. The presence of Cd, La and S signals can be observed in the survey spectrum (Fig. 2a), as well as the adventitious C and O impurity, which can be attributed to the graphite conductive adhesive or the absorbed gaseous molecules. Fig. 2b shows the high–resolution XPS spectrum of the Cd 3d. The peaks located at the binding energy of 405.0 and 411.8 eV with a spin − orbit splitting energy of 6.8 eV can be ascribed to the Cd $3d_{5/2}$ and $3d_{3/2}$ of $Cd^{2+}$ state, respectively. Two pairs of La 3d peaks located around (835.3, 839.2) and (852.0, 855.8 eV) can be observed in Fig. 2c, which can be attributed to the La $3d_{5/2}$ and La $3d_{3/2}$, respectively. The satellite peaks are present a 3.9 eV higher binding energy than the main peaks. The spin–orbit splitting of La $3d_{5/2}$ and La $3d_{3/2}$ is *ca.* 16 eV demonstrating the $La^{3+}$ state in $CdLa_2S_4$. This finding is consistent with the previous works. [47,50]. The binding energies of S $2p_{3/2}$ and S $2p_{1/2}$ (Fig. 2d) were determined to be 161.3 and 162.4 eV, respectively, revealing a normal state of $S^{2-}$. The atomic ratio of Ca, La, and S was determined by the XPS peak areas after correcting the sensitivity factors of the elements and the result (Ca: La: S) is 1:1.9:3.6, a value close to the theoretical stoichiometry of $CdLa_2S_4$.

### 3.2. Photocatalytic activities

Photocatalytic SO of p–MBA to p–MBAD and SR of NB to AL on $CdLa_2S_4$ in one reaction system was investigated under visible light irradiation ($\lambda > 420$ nm) in $N_2$ atmosphere. Two blank tests without the photocatalyst or light irradiation were first performed and the results indicated that the SO or SR reactions cannot occur, which confirm that the reactions were truly driven by a photocatalytic process. Fig. 3 shows the variation of the conversion (C%) of the reactants and the selectivity (S%) and the yield (Y%) of the products formed with irradiation time. For the SR of NB, besides the final product of AL, the intermediate reduction product NSB was also observed. The formations of p–MBAD, NSB, and AL were confirmed by GC–MS analysis as shown in Fig. S2 and their amounts were determined by GC (a typical GC chromatogram is shown in Fig. S3). As shown in Fig. 3, the C% of p–MBA (Fig. 3a) and NB (Fig. 3b) first increases with irradiation time and then approach a stable value 4 h later. After irradiation for 10 h, a maximum C% of *ca.* 90% and 100% can be achieved for p–MBA and NB, respectively. Similar variation tendencies can be found for the generation of p–MBAD and AL. After irradiation for 10 h, the Y% of p–MBAD and AL is 78.6% and 55.9%, respectively.

For the SR of NB, the yield of NSB ($Y_1$%, Fig. 3) is more significant than AL ($Y_2$%) in the initial reaction stage, which suggests that the reduction of NB to NSB is more reactive than NSB to AL. An accumulation of NSB is then present. However, when all NB was consumed (about 4 h later), a decay of NSB can be observed, meanwhile AL increases continuously, implying a further conversion of NSB to AL is

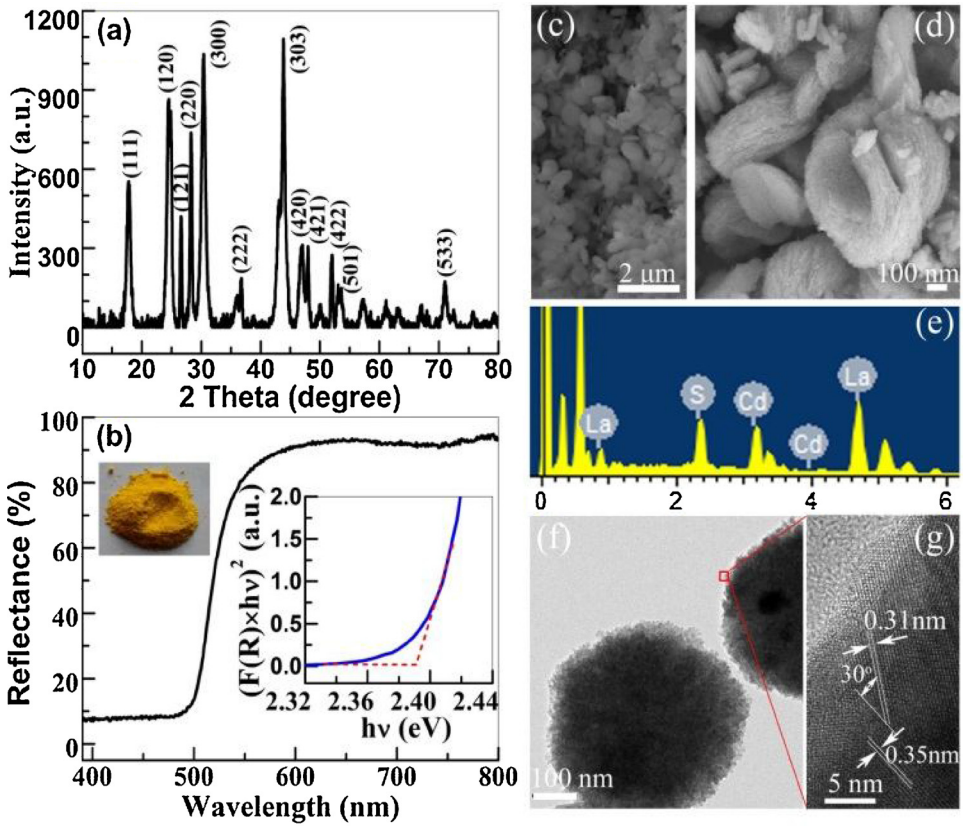


**Fig. 1.** Some characterization results of the prepared $CdLa_2S_4$: (a) XRD pattern; (b) UV–vis DRS. The inset is the image of the sample (left) and the Tauc plots (right) of the transformed Kubelka–Munk function $(F(R) \times h\nu)^2$ vs. $h\nu$; (c and d) SEM images; (e) EDS result; (f) TEM and (g) HRTEM images.

occurred. As both NSB and AL are the reduction products of NB, the sum of their amount was used to calculate the overall selectivity and yield (line of $(Y_1 + Y_2)$%) of the SR of NB in Fig. 3b. Both the S% of p–MBAD and NB first increase with irradiation time and then decrease with time further prolonged. A maximum S% of 98.8% and 96.1% was observed for the formation of p–MBAD and the sum of NSB and AL, respectively. The reduction of the selectivity after irradiation for 4 h suggests a further conversion of the target products. Thus, the optimal reaction time for the selective conversions of p–MBA and NB is 4 h. As shown in Fig. 3, the SO and SR exhibit the same variation profiles in the conversion, yield and selectivity, which implies that a coupling of the two reactions was reached on $CdLa_2S_4$. After irradiation for 4 h, the ratio of $h^+$/e– used for the SOTs was calculated based on the products' amounts (*i.e.* p–MBAD, NSB and AL) and the result is *ca.* 1.15:1 (See the supporting information for the calculation procedure), demonstrating a synergistic effect between the two semi–conversions.

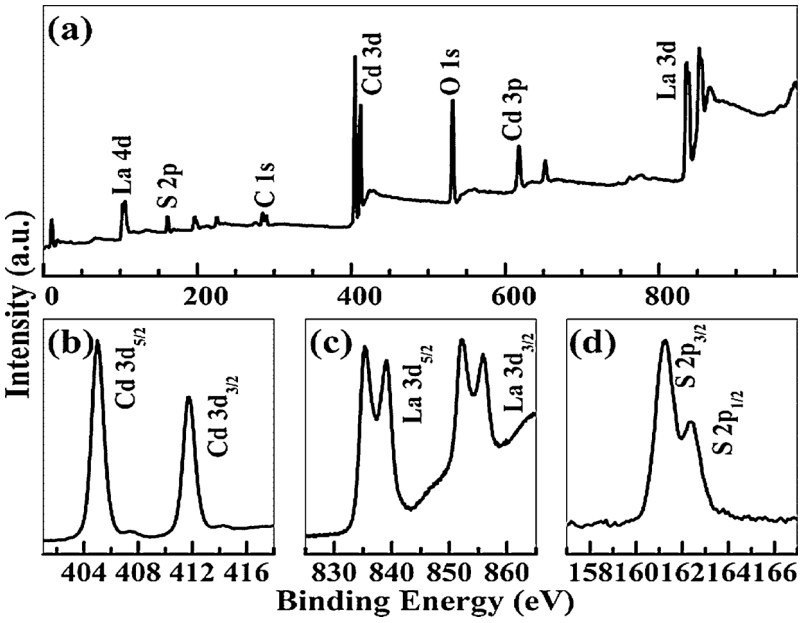


**Fig. 2.** (a) survey and high resolution (b) Cd 3d, (c) La 3d, and (d) S 2p XPS spectra of the prepared $CdLa_2S_4$.

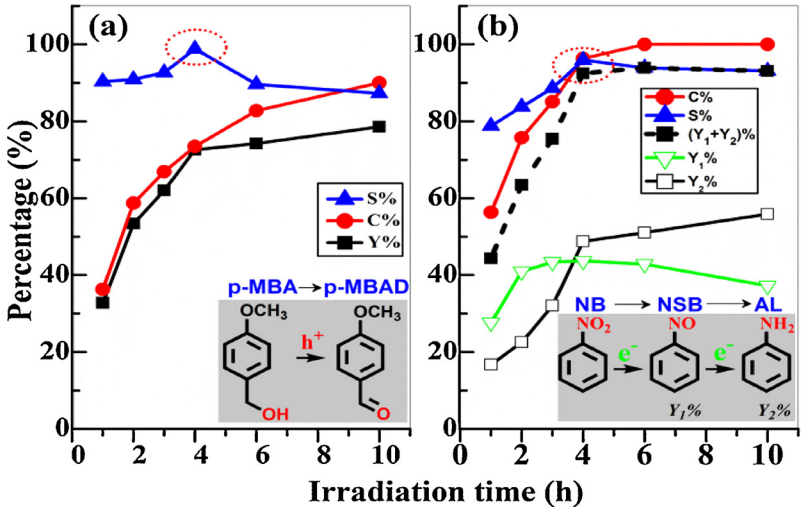


**Fig. 3.** The variation of the conversion (C%) of the reactants and the selectivity (S%) and the yield (Y%) of the products with the irradiation time in (a) SO of p–MBA to p–MBAD and (b) SR of NB to AL in one reaction system.

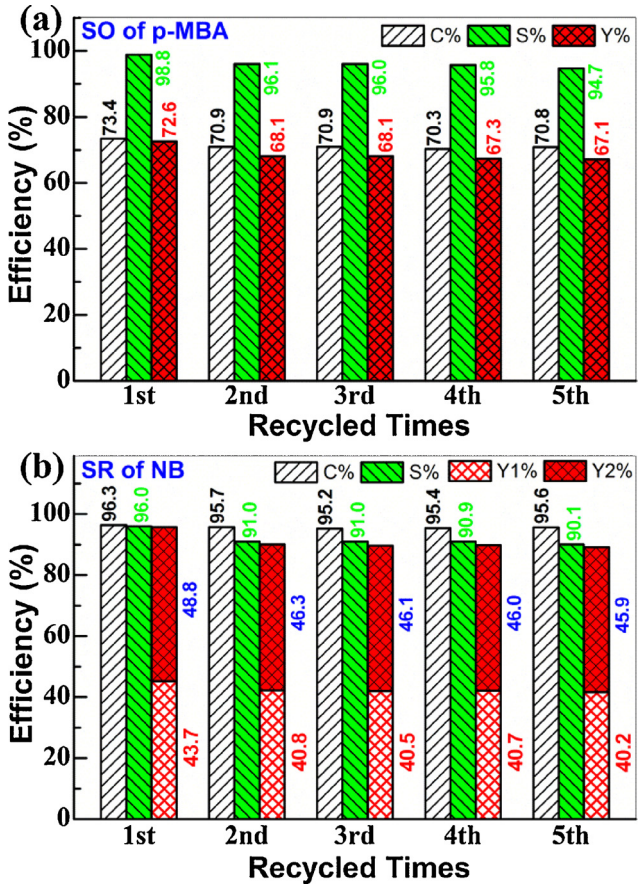


**Fig. 4.** Recycled testing of the photocatalytic activity of $CdLa_2S_4$ for the (a) SO of p–MBA and (b) SR of NB under visible light irradiation for 4 h.

Reusing $CdLa_2S_4$ for the selective conversion of p–MBA and NB was performed for 5 runs to assess the stability of $CdLa_2S_4$. As shown in Fig. 4, a quite stable performance of $CdLa_2S_4$ can be observed. The standard deviation of the results is within 3%. The conversion of p–MBA and the yield of p–MBAD are around 71.3% and 68.6%, respectively, corresponding to a selectivity about 96.3%, while the conversion of NB and the yields for NSB and AL are *ca.* 95.6%, 41.2% and 46.6%, respectively, corresponding to an overall selectivity about 91.8%. The high selectivity of the coupled–reaction system and the photocatalytic stability of $CdLa_2S_4$ can be largely approved by the cyclic test. The XRD patterns of the fresh and the used $CdLa_2S_4$ for 5 runs test are shown in Fig. S4. Apparently, the used sample shows an identical XRD pattern to the fresh one, further confirming the stability of $CdLa_2S_4$.

To further investigate the generality of $CdLa_2S_4$ for the photocatalytic SOTs in one reaction system, the conversions of other p–substituted aromatic alcohols and nitroarenes were conducted. The substituted groups in the aromatic alcohols and nitroarenes were denoted as X– and Y–, respectively. After irradiation for 4 h, the conversion parameters were summarized in Table 1. The effect of the p–substituted groups on the SO or SR reaction was first investigated with the other half reaction stabilized. As shown in entry 1–4, for the effect of X–, the conversion of aromatic alcohols and the yield of the corresponding aldehydes decrease in order $H_3CO-$ > H– > Cl– > F–, which is opposite from the electronegativity order of the p–function groups $H_3CO-$ < H– < Cl– < F–. Although a slight decrease of the selectivity is observed, the values are still higher than 90%. Apparently, the electron–donating substituent in the para position (*i.e.* $-OCH_3$) rather than the electron–withdrawing groups (–F, and –Cl) benefits the SO of $-CH_2OH$ to –CHO because the electron density of $-CH_2OH$ can be improved. This finding agrees well with the reported results [30,37,39]. As the SR of NB is associated with the SO of aromatic alcohols, its conversion and the yield of NSB and AL also retarded by the electron–withdrawing groups. However, with change the electron–donating group to –withdrawing groups, the selectivity of NB decreased dramatically from 96.1% to only ca. 30%. It seems that the presence of electron-withdrawing groups are detrimental to the SR of NB to AL, even they locate at the benzyl alcohols. These groups lead to the conversion of NB to other intermediate rather than NSB or AL.

According to Ferry's work [13], the intermediate should be N–phenylhydroxylamine. The reduction of nitro group to amine is a sequential $H^+$–coupled six e—reduction process. The conversion not only determined by the deprotonation of aromatic alcohols (providing $H^+$), but also the utilization of photoinduced $e^-$. It is a complex and kinetically unfavourable process. Beside anilines, other intermediates or products including nitroso [13,15,19,51–53] (two e—reduction product), N-phenylhydroxylamine [13,19,52] (four e—reduction product), azo and azoxy compounds formed between nitroso and N-phenylhydroxylamine or anilines [19,53,54] may also be produced with the reduction proceeding. These intermediates have been observed in some reported works [13,15,19,51–53] and partially confirmed by the GC–MS results as shown in Figure S5 in the supporting information. At present, due to the limitation of the GC determination method, only one

**Table 1**
Photocatalytic conversion of other p–substituted aromatic alcohols and nitroarenes on $CdLa_2S_4$ under visible light irradiation for 4 h.

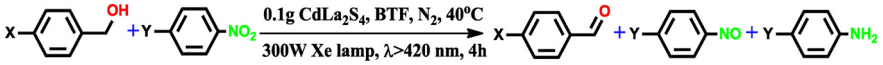


| Entry | X– | Y– | SO reactions | | | SR reactions | | | | $R_{h+/e-}$ |
|---|---|---|---|---|---|---|---|---|---|---|
| | | | C% | S% | Y% | C% | S%[a] | $Y_1$%[b] | $Y_2$%[c] | |
| 1 | $H_3CO$– | H– | 73.5 | 98.8 | 72.7 | 96.3 | 96.1 | 43.7 | 48.8 | 1.15:1 |
| 2 | H– | H– | 62.4 | 92.5 | 57.7 | 79.8 | 32.6 | 10.2 | 15.8 | 3.01:1 |
| 3 | Cl– | H– | 61.1 | 90.8 | 55.5 | 75.2 | 31.8 | 10.0 | 13.9 | 3.22:1 |
| 4 | F– | H– | 51.9 | 90.3 | 46.8 | 73.8 | 28.2 | 9.8 | 11.0 | 3.30:1 |
| 5 | $H_3CO$– | Cl– | 61.4 | 90.9 | 55.8 | 90.2 | 30.6 | 8.7 | 18.9 | 2.56:1 |
| 6 | $H_3CO$– | $H_3C$– | 51.0 | 92.3 | 47.1 | 66.0 | 36.7 | 9.6 | 14.6 | 2.64:1 |
| 7 | $H_3CO$– | F– | 62.4 | 91.2 | 56.9 | 90.5 | 33.7 | 10.2 | 20.3 | 2.40:1 |
| 8 | H– | $H_3C$– | 52.9 | 86.4 | 45.7 | 64.9 | 30.9 | 6.7 | 13.4 | 2.92:1 |
| 9 | Cl– | F– | 60.9 | 91.6 | 55.8 | 78.2 | 23.4 | 5.8 | 12.5 | 3.86:1 |
| 10 | F– | Cl– | 56.0 | 89.6 | 50.2 | 76.8 | 35.7 | 10.5 | 16.9 | 2.46:1 |
| 11 | H– | Cl– | 62.5 | 93.9 | 58.7 | 80.3 | 36.9 | 10.9 | 18.7 | 2.63:1 |
| 12[d] | $H_3CO$– | H– | 61.0 | 80.3 | 48.9 | 75.3 | 15.2 | – | 11.4 | 4.29:1 |
| 13[e] | $H_3CO$– | H– | 61.0 | 90.3 | 55.0 | 75.3 | 39.5 | – | 29.7 | 1.85:1 |

[a] estimated based on nitroso and aniline compounds.
[b] yields of the nitroso compounds.
[c] yields of the amines.
[d] test performed on CdS nanorods.
[e] test performed on CdS nanorods and the product of Schiff base was taken into the calculations.

of the intermediates (nitroso) and the full reduction product (aniline) have been measured in this work. When electron-withdrawing groups are present in the reaction system, the electron density around nitrogen will be increased by the inductive effect of the groups during the hydroxylamine step, which makes a further reduction of hydroxylamine is less favourable [13]. A full reduction of nitro to amine is then hindered and the reduction then ends at the N-phenylhydroxylamine step. As a result, a low selectivity of NB to NSB and AL is then present in the presence of electron-withdrawing groups. This is consistent with the reported observations [1334,55,56].

Entry 1 and 5–7 shows the effect of the Y– on the selective conversions. With change of Y– from H– to other groups (Cl–, F–, $H_3C$–), both the SR and SO conversions decrease substantially, especially for $H_3C$–. The significant suppression of $H_3C$– on the SR of nitro group also has been observed in Füldner's work [57]. The result suggests the existence of a steric hindrance effect, which leads to a sharp decrease of the SR selectivity from 96.1% to only *ca.* 35%, as well as the reduction of the yields. It may be caused by the fact that a large Y– group is not in favor of the absorption of nitroarenes on $CdLa_2S_4$. As e– cannot be effectively involved in the SR reactions, the $h^+$–induced SO reactions are also retarded. However, the selectivity of the SO is almost not impacted by the change of Y– groups and remains *ca.* 91.0%. This suggests that, although the SO and SR conversions are interacted on each other, the selectivity from p–MBA to p–MBAD is independent of the SR reactions. The steric hindrance effect of Y– groups mainly influences the reduction of nitro group rather than the oxidation of hydroxyl group. For –Cl and –F substituted nitroarenes, the GC and GC–MS (Fig. S5) results indicated that no dehalogenation has been occurred. The photoinduced e– is mainly involved in the reduction of nitro group rather than of Cl– and F–. This is consistent with the reported works [16,29,31,58]. Similar to the result observed in entry 1–4, the full reduction of nitro groups to the corresponding amines are also disturbed by the electron-withdrawing groups as the selectivities are substantially reduced. Besides, the detrimental effects of the high electronegative X– groups on the SO and the large Y– groups on the SR conversions can be further perceived in entry 8–11.

As shown in the last column of Table 1, the ratios of $h^+$/e– ($R_{h+/e-}$) involved in the selective conversions are significantly larger than 1 except the entry 1. It suggests that, although the SO and SR conversions can be achieved simultaneously on $CdLa_2S_4$, $h^+$-induced SO of aromatic alcohols is more reactive than the e–-induced SR of nitroarenes. Although some photoinduced e– may be involved in the reduction of $H^+$ to form $H_2$ [47,49,50,59], the competing reaction is not the main reason lead to $R_{h+/e-}$ larger than 1 because a large number of nitro group did participate in the conversion reaction as shown in Table 1. As only one of the intermediates (nitroso) and aniline have been measured in this work due to the limitation of the GC determination method, the amount of $e^-$ involved in the reduction of nitro group is actually underestimated. This is the main factor lead to the values of $R_{h+/e-}$ is greater than 1.

Our group recently reported that [34] the SO benzyl alcohol into benzaldehyde and SR of nitrobenzene into aniline can be achieved on $CdIn_2S_4$ photocatalyst and the reactions of entry 1–4 in Table 1 have been measured. Here, we must point that, compared with $CdIn_2S_4$, the as-synthesized $CdLa_2S_4$ photocatalyst exhibits apparent higher photocatalytic performance for the redox conversions in a coupled reaction system. In addition, not only the oxidation substrate, but also the reduction substrates have been extended in this work to investigate the generality of $CdLa_2S_4$ for the photocatalytic SOTs in one reaction system.

CdS is a well–known visible light photocatalyst and our previous work indicated that SO of p–MBA and SR of NB also can be realized on CdS [30,39]. Furthermore, Cd and S are the constitutes of $CdLa_2S_4$. Thus, the performance of CdS for SOTs was then investigated to compare its activity with $CdLa_2S_4$. Hexagonal CdS nanorods (as indicated by Fig. S6) which commonly show high photocatalytic performance [39] were prepared intentionally. As shown in the entry 12 in Table 1, for the SO of p–MBA, the conversion of p–MBA and the yield of p–MBAD are only 61.0% and 48.9%, respectively, corresponding to a selectivity of 80.3%, while as for the SR of NB, the conversion of NB and the yield of AL are 75.3% and 11.4% respectively, corresponding to a selectivity of 15.2%. Apparently, the activity of CdS is substantially lower than that of $CdLa_2S_4$ (entry 1). Unlike $CdLa_2S_4$, no any NSB was observed during the reaction. However, Schiff base which yielded from the reaction between the products of AL and p–MBAD was observed in CdS reaction system by the GC and GC-MS (Fig. S7). If this product is taken into the calculations of the SO and SR performances, the selectivity of the SO and the yield of p–MBAD should be 90.3% and 55.0%, respectively, while the selectivity of the SR and the yield of AL are 39.5% and 29.7% (entry 13). The revised activity of CdS is still lower than that of

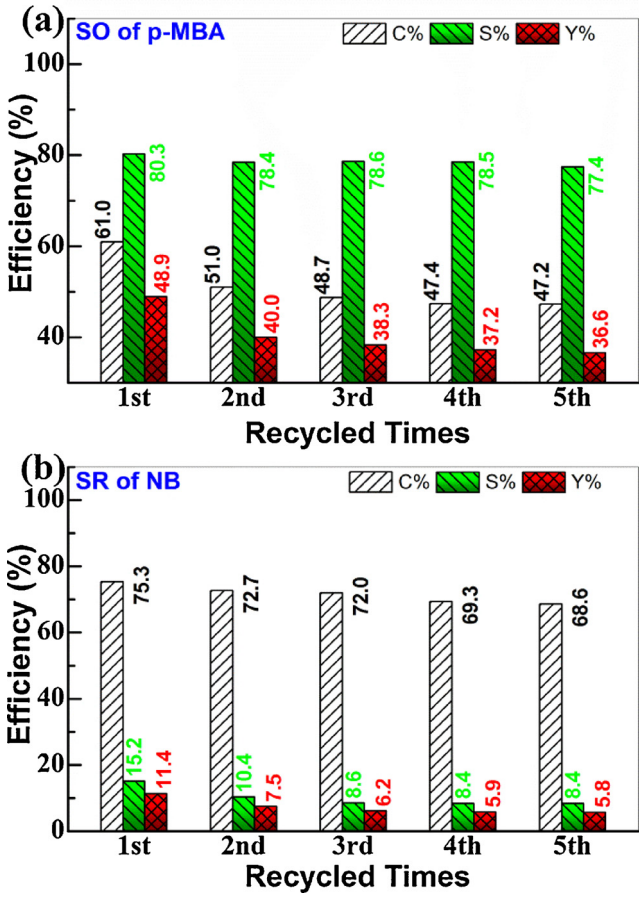


**Fig. 5.** Recycled testing of photocatalytic activity of CdS for the (a) SO of p–MBA to p–MBAD and (b) SR of NB to AL under visible light irradiation for 4 h.

$CdLa_2S_4$. The low efficiency of CdS for the conversion of other alcohols and the detrimental effects of the high electronegative X– groups on the SO performance can be further observed in Table S1.

Besides the activity, the stability of CdS is also inferior to that of $CdLa_2S_4$. As shown in Fig. 5, a gradual deactivation of CdS can be perceived with recycle time. The deactivation of CdS may be caused by the photocorrosion of CdS [45,60]. The higher activity and the stability of $CdLa_2S_4$ than that of CdS also have been observed for photocatalytic $H_2$ production [47].

The inferior performance of CdS can be mainly ascribed to two factors. First, the BET surface area of CdS is only 5.8 $m^2/g$, while the area of prepared $CdLa_2S_4$ is as high as 48.9 $m^2/g$. A photocatalyst with a high surface area can harvest more irradiation light and provides more active sites for the photocatalytic reaction which eventually occurs on the surface. Second, compared to $CdLa_2S_4$, CdS shows a lower efficiency for the separation of photoinduced charge carriers. Electrochemical impedance spectroscopy (EIS) is a very useful tool to characterize the interfacial charge transferring performance. As shown in Fig. 6a, the Nyquist plot of $CdLa_2S_4$ shows a smaller arc radius at a high frequency than that of CdS, suggesting $CdLa_2S_4$ has a smaller electric resistance. Thus, a faster transport of charge carriers and more effective e—$h^+$ separation can be achieved on $CdLa_2S_4$. Besides EIS, the recombination of photoinduced charge carriers was investigated by PL spectra at room temperature with an excitation wavelength of 400 nm. Generally, a weak PL intensity indicates a low recombination rate of e– and $h^+$ [45,61]. As indicated in Fig. 6 b, a strong emission around 538 nm can be observed on both of CdS and $CdLa_2S_4$. The PL peak intensity of $CdLa_2S_4$ is obviously weaker than that of CdS, indicating that the recombination rate of charge carriers in $CdLa_2S_4$ is lower than that

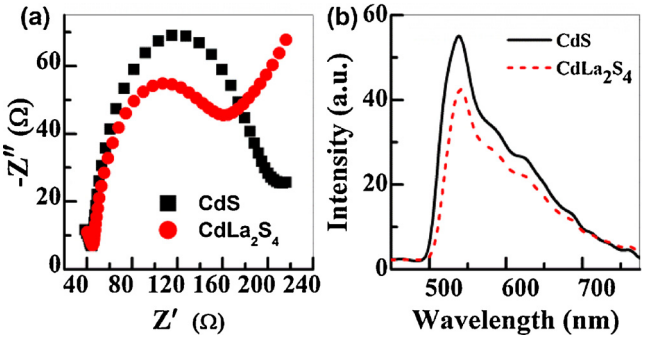


**Fig. 6.** (a) EIS Nyquist plots of CdS and $CdLa_2S_4$. (b) Photoluminescence (PL) spectra of CdS and $CdLa_2S_4$ with an excitation wavelength of 400 nm at room temperature.

in CdS. The result further confirms that $CdLa_2S_4$ has high efficiency for the separation of photogenerated charge carriers. Thus, unlike CdS, the photocorrosion of $CdLa_2S_4$ will be suppressed, which is commonly induced by the trapped charge carriers. We believe that these advantages lead to the high stability of $CdLa_2S_4$. The high stability of $CdLa_2S_4$ for other photocatalytic reactions also has been confirmed by experimental investigations [47–49,62].

### 3.3. Conversion mechanism

To investigate the coupling mechanism of the SO and SR reactions over $CdLa_2S_4$, the oxidation potentials of p–MBA and p–MBAD and the reduction potentials of NB and NSB were measured by CV. As shown in Fig. 7, the redox potentials of the substrates are independent on their concentrations. The voltammogram of p–MBA exhibits an irreversible curve and two oxidative potentials can be observed (Fig. 7a). In details, the first oxidative potential is *ca.* +1.60 V (vs Ag/AgCl, similarly hereinafter) and it can be assigned to the oxidation of p–MBA to p–MBAD, while the second one locates at *ca.* +2.02 V and it can be ascribed to the further oxidation of p–MBAD to p–methoxybenzoic acid [8]. The latter assumption was further confirmed by the voltammogram of p–MBAD in Fig. 7b. Fig. 7c and d show the voltammogram of NB and NSB and the results indicate that the reductive potentials of NB to NSB, and NSB to AL are –0.69 V and –0.71 V, respectively, agreeing well with our previous findings [34,39]. Therefore, the request of CB and VB edges of the potential photocatalyst for the coupling of SO of p–MBA to

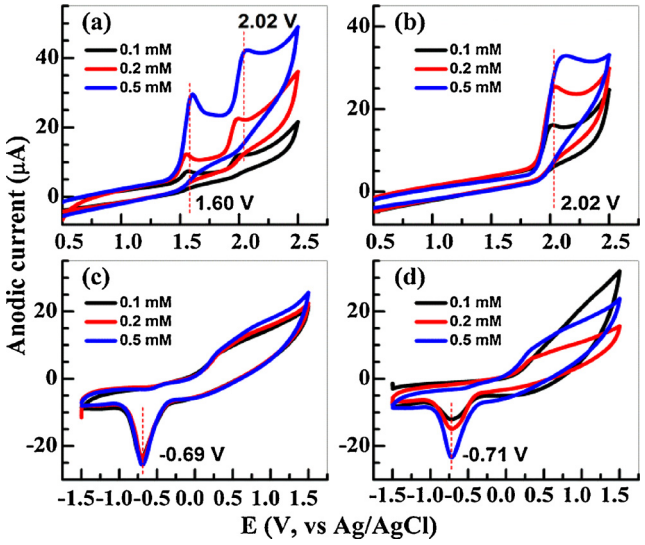


**Fig. 7.** The CV of (a) p–MBA, (b) p–MBAD, (c) NB and (d) NSB with a concentration of 0.1, 0.2, and 0.5 mM.

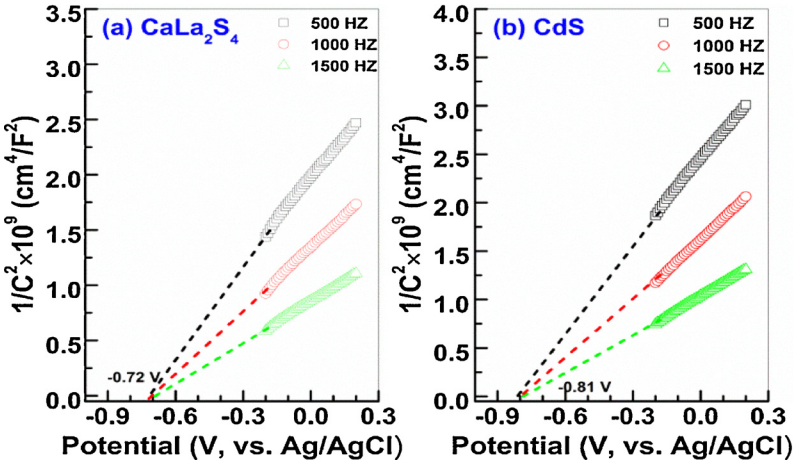


**Fig. 8.** Mott–Schottky plots of the prepared (a) $CdLa_2S_4$ and (b) CdS.

p–MBAD and SR of NB to AL can be derived according to the CV results. It suggests that, thermodynamically, the conduction band bottom potential ($E_{cb}$) of the candidate photocatalyst should be more negative than –0.71 V, while the valence band top potential ($E_{vb}$) should be in the range of 1.60–2.02 V to trigger the conversion and avoid a deep–oxidation.

To determine whether the band structures of the prepared $CdLa_2S_4$ and CdS meet the thermodynamical request shown in Fig. 7, the CB edges of the samples were evaluated by Mott–Schottky analysis. As shown in Fig. 8, the positive slopes of the plots demonstrate a n–type characteristic semiconductor of the prepared $CdLa_2S_4$ and CdS [63,64]. The $V_{fb}$ values of $CdLa_2S_4$ and CdS are estimated from the extrapolation of the lines to the intercept of x axis and the results indicate that the $V_{fb}$ of $CdLa_2S_4$ is –0.72 V (vs. Ag/AgCl), while the value of CdS is –0.81 V. As the $E_{fb}$ is approximate to the $E_{cb}$, the band structure of the $CdLa_2S_4$ and CdS then can be constructed based on the $E_{fb}$ and the $E_g$ of the samples. The $E_{vb}$ of $CdLa_2S_4$ and CdS is calculated to be 1.67 and 1.61 V, respectively. Obviously, in theory, the SO and SR reactions can be proceeded simultaneously on both of $CdLa_2S_4$ and CdS. The $E_{vb}$ values of $CdLa_2S_4$ and CdS ensure that the oxidation of p–MBA to p–MBAD can occur, but a further oxidation to p–methoxybenzoic acid is prohibited because the potential is lower than the oxidation potential of p–MBAD to p–methoxybenzoic acid (2.02 V). However, the further reduction of NSB to AL is hampered on $CdLa_2S_4$ as its $E_{cb}$ is slightly lower than the reduction potential of NSB to AL. Thus, the conversion of NSB to AL is the rate–determining step for the SR of NB and the intermediate of NSB then can be accumulated and detected by GC as shown in Fig. 3. However, as the $V_{cb}$ of CdS is as low as –0.81 V, the reduction of NSB to AL can readily occur on CdS and no accumulation of NSB then can be observed. Thus, consistent with the experimental results, the CV and Mott–Schottky analysis also suggests that the SO of p–MBA to p–MBAD and SR of NB to AL can be achieved simultaneously on $CdLa_2S_4$ and CdS under visible light irradiation and the selectivity of the conversions is mainly determined by their band structures.

To further investigate the coupling mechanism between the SO of p–MBA to p–MBAD and SR of NB to AL, the potential active species that are responsible for the conversions were analyzed by a series of controlled experiments with $CCl_4$ (10 μL) and triethanolamine (TEOA, 2 μL) as scavengers to trap the photogenerated e– and $h^+$, respectively [12,65]. As shown in Fig. 9a, for $CCl_4$ added test, compared to the reaction coupled in $N_2$ atmosphere, the conversion and the selectivity of the SR decreased significantly from 96.3% and 96.0% to 78.9% and 65.1%, respectively, while the yields of NSB and AL are only 21.4% and 24.7%. It suggests that the photogenerated e– is responsible for the reduction of NB to AL. Meanwhile, as shown in Fig. 9b, the SO performance is slightly improved due to the trapping of e– by $CCl_4$, which

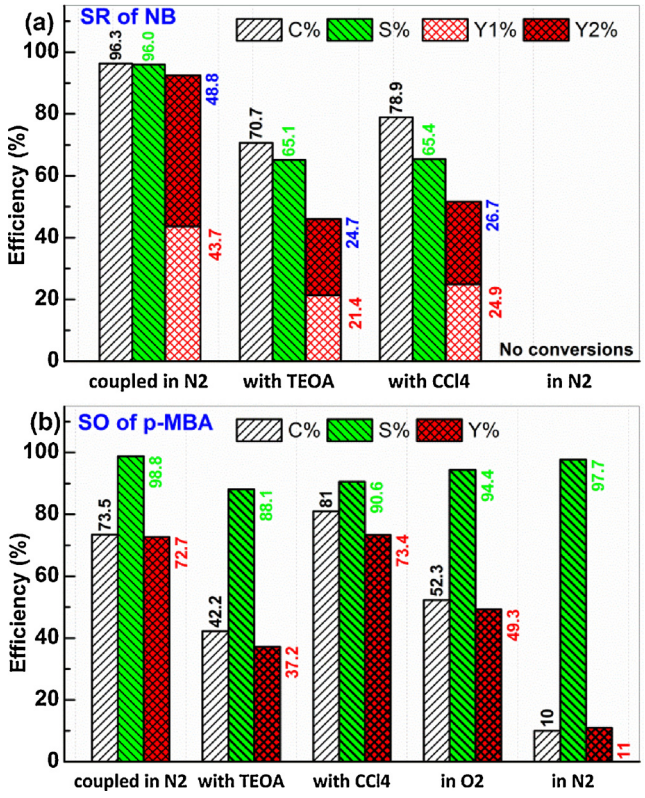


**Fig. 9.** (a) The SR of NB and (b) SO of p–MBA performances on $CdLa_2S_4$ in a coupled reaction model with $CCl_4$ and TEOA as scavengers or in a separated reaction model in $N_2$ or $O_2$ atmosphere.

benefits the SO of p–MBA. Considering that the reaction is performed in BTF, the oxidation of p–MBA is more likely triggered directly by photoinduced $h^+$ rather than by ·OH due to the lack of $H_2O$. To confirm this assumption, TEOA, a commonly used hole scavenger was added into the solution and the results indicated that the SO performance was substantially reduced. The conversion of p–MBA and the yield of p–MBAD decreased from 73.5% and 72.6% to only 42.2% and 37.2%, respectively. Surprisingly, although $h^+$ was captured by TEOA, the SR conversion induced by e– was not improved consequently and the activity is even lower than the test with $CCl_4$ added (Fig. 9b). It confirms that the SR conversion relies on the activity of SO as the reduction of nitro group is dependent on the availability of e– and the amount of $H^+$ deprotonated from p–MBA. Both $H^+$ and e– are involved in the SR of NB. A further control test with both of $CCl_4$ and TEOA as e– and $h^+$

scavengers, respectively, has been added. The result indicated that only trace amount of AL is produced and the yield of p-MBAD is only 3.6% (Fig. S8). It suggests that the SOT conversions were truly induced by photogenerated e– and $h^+$. These findings demonstrate that the half conversions not only be coupled by the photoinduced e– and $h^+$, but also collaborate with each other through $H^+$.

The SO of p–MBA and SR of NB were carried out separately in $O_2$ or $N_2$ atmosphere to further corroborate their synergistic mechanism and highlight the advantage of the coupled reaction system. As shown in Fig. 9b, although the selectivity of p–MPA is less affected, the conversion of p–MBA and the yield of p–MBAD in $O_2$ or $N_2$ are obviously lower than that performed in the coupled reaction system, especially for the reaction carried out in $N_2$. The low SO efficiencies should be restricted by the other half reaction, *i.e.* the consuming of the photoinduced e–. Due to the low solubility of $O_2$ in BTF and the absence of the cocatalyst on $CdLa_2S_4$, e– cannot be effectively involved in the reduction of $O_2$ or $H^+$ (originated from the deprotonation of p–MBA by photoinduced $h^+$). However, the consumption of e– is easy to be proceeded with the soluble NB. This is the reason why the coupled system shows higher performance for SO of p–MPA than that performed separately in $O_2$ or $N_2$. The indispensability of $H^+$ source for the SR of NB was further confirmed by the reaction performed separately in $N_2$ (as shown in Fig. 9a). No conversion of NB was observed due to the lack of $H^+$ source.

Thus, it can be drawn that the SO of p–MBA can be carried out independently in $O_2$ or $N_2$ or in combination with the SR of NB. $H^+$ deprotonated from p–MBA by $h^+$ can be reduced to $H_2O$ in an $O_2$–enriched environment or to $H_2$ in an anoxic environment. For the tests performed in $O_2$ and $N_2$, the corresponding reduction products of $H_2O$ and $H_2$ have been qualitatively detected as shown in Fig. S9. However, the SR of NB can only occur with the participation of e– and $H^+$. Thus, coupling the SO of p–MBA and SR of NB in one photocatalytic reaction system is an ideal scenario to improve both the conversion and the quantum efficiency for SOTs, even though most of the SR conversions are still unsatisfactory as shown in Table 1.

Based on the above results and some reported reaction mechanism, the coupling mechanism between the photocatalytic SO of aromatic alcohols and SR of nitroarenes is proposed and illustrated in Scheme 1. Photogenerated e– and $h^+$ pairs can be formed on $CdLa_2S_4$ under visible light irradiation. SO of the $–CH_2(OH)$ to –CHO is then mediated by a $h^+$ dominated oxidation route along with a successive deprotonation (process a, Scheme 1) [7,8,12,28,66,67]. A further oxidation of –CHO to –COOH is prohibited by the low $E_{vb}$ of $CdLa_2S_4$. Two $h^+$ is consumed for the conversion of one molecule of the alcohols and meanwhile two $H^+$ are produced. The $H^+$ then reacts with the nitro groups to form nitroso, hydroxylamine and amine compounds via a two–, four–, and six–electron reduction process (process b, Scheme 1) [13,15,68–70]. As the SR of nitro group to aniline involves a six sequential proton-coupled e– transfer steps, the conversion will be determined not only by the deprotonation efficiency of aromatic alcohols, but also the utilization of photoinduced e–. Compared to SO of aromatic alcohols, the SR conversion is essentially a complex and kinetically unfavorable process.

## 4. Conclusions

In summary, a novel $CdLa_2S_4$ photocatalyst was synthesized by a facile solvothermal method. Coupling the visible–light–induced SO of aromatic alcohols and SR of nitroarenes in one reaction system was achieved successfully on $CdLa_2S_4$ in $N_2$ atmosphere. The sample shows high stability and good generality for the conversions due to the well–matched band structure and the high separation efficiency of photoinduced e– and $h^+$. The electro–donating substituent in the para position ($-OCH_3$) rather than the withdrawing groups (−F, and −Cl) benefit the SO of aromatic alcohols to aldehydes and the selectivities are as high as *ca.* 90%. For p–substituted nitroarenes, the SR to the corresponding anilines is vulnerable to the electron–withdrawing groups and the steric hindrance of the p–substituent and the selectivities are significantly lower than that of the SO conversions. The SO reactions were triggered by $h^+$ via a successive deprotonation, while the SR conversions were achieved by a $H^+$–coupled six e– reduction process. The SO and SR conversions are not only coupled by the photoinduced e– and $h^+$, but also collaborate with each other by $H^+$. This work reveals that $CdLa_2S_4$ is a good candidate to couple the SO and SR conversions in one reaction system, which is an ideal scenario to improve both the conversion and the quantum efficiency for selective transformation of organics.

## Acknowledgements

This work was financially supported by the National Natural Science Foundation of China (NSFC, Grant Nos. 21525313, 51472005, 21473066, 51772118, 21607027 and 21603002) and the Natural Science Foundation of Anhui Province (Grant Nos. 1608085QB37).

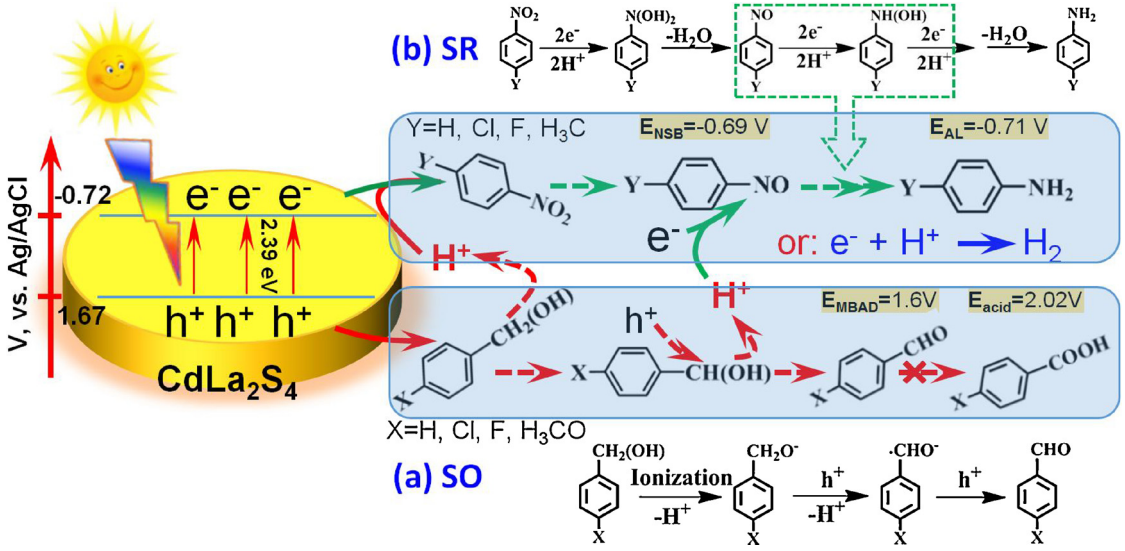


**Scheme 1.** Proposed schematic mechanism for the coupling of photocatalytic SO of aromatic alcohols and SR of nitroarenes on $CdLa_2S_4$ under visible light irradiation.

Prof. Xianliang Fu thanks the support from the Outstanding Youth Foundation of Anhui Province (No. 1808085J24).

## Appendix A. Supplementary data

Supplementary material related to this article can be found, in the online version, at doi:https://doi.org/10.1016/j.apcatb.2018.03.084.

## References

[1] Y. Shiraishi, T. Hirai, J. Photochem. Photobiol. C 9 (2008) 157–170.
[2] M.Q. Yang, Y.J. Xu, Phys. Chem. Chem. Phys. 15 (2013) 19102–19118.
[3] X. Lang, X. Chen, J. Zhao, Chem. Soc. Rev. 43 (2014) 473–486.
[4] S. Munir, D.D. Dionysiou, S.B. Khan, S.M. Shah, B. Adhikari, A. Shah, J. Photochem. Photobiol. B Biol. 148 (2015) 209–222.
[5] Y. Zheng, L. Lin, B. Wang, X. Wang, Angew. Chem. Int. Ed. 54 (2015) 12868–12884.
[6] M. Zhang, C. Chen, W. Ma, J. Zhao, Angew. Chem. Int. Ed. 47 (2008) 9776–9879.
[7] F. Su, S.C. Mathew, G. Lipner, X. Fu, M. Antonietti, S. Blechert, X. Wang, J. Am. Chem. Soc. 132 (2010) 16299–16301.
[8] S. Higashimoto, N. Suetsugu, M. Azuma, H. Ohue, Y. Sakata, J. Catal. 274 (2010) 76–83.
[9] Y. Chen, J. Zhang, M. Zhang, X. Wang, Chem. Sci. 4 (2013) 3244–3248.
[10] S. Higashimoto, R. Shirai, Y. Osano, M. Azuma, H. Ohue, Y. Sakata, H. Kobayashi, J. Catal. 311 (2014) 137–143.
[11] H. Li, F. Qin, Z. Yang, X. Cui, J. Wang, L. Zhang, J. Am. Chem. Soc. 139 (2017) 3513–3521.
[12] X.Y. Xiao, J. Jiang, L.Z. Zhang, Appl. Catal. B 142 (2013) 487–493.
[13] J.L. Ferry, W.H. Glaze, Langmuir 14 (1998) 3551–3555.
[14] H. Tada, T. Ishida, A. Takao, S. Ito, Langmuir 20 (2004) 7898–7900.
[15] S.O. Flores, O. Rios-Bernij, M.A. Valenzuela, I. Córdova, R. Gómez, R. Gutiérrez, Top. Catal. 44 (2007) 507–511.
[16] K. Imamura, K. Hashimoto, H. Kominami, Chem. Commun. 48 (2012) 4356–4358.
[17] L. Yuan, M.-Q. Yang, Y.-J. Xu, J. Mater. Chem. A 2 (2014) 14401.
[18] C. Han, Z. Chen, N. Zhang, J.C. Colmenares, Y.-J. Xu, Adv. Funct. Mater. 25 (2015) 221–229.
[19] Q. Xiao, Z. Liu, F. Wang, S. Sarina, H. Zhu, Appl. Catal. B 209 (2017) 69–79.
[20] C.P. Vinod, K. Wilson, A.F. Lee, J. Chem. Technol. Biotechnol. 86 (2011) 161–171.
[21] K. Mori, T. Hara, T. Mizugaki, K. Ebitani, K. Kaneda, J. Am. Chem. Soc. 126 (2004) 10657–10666.
[22] K. Yamaguchi, K. Mori, T. Mizugaki, K. Ebitani, K. Kaneda, J. Am. Chem. Soc. 122 (2000) 7144–7145.
[23] A. Agrawal, P.G. Tratnyek, Environ. Sci. Technol. 30 (1996) 153–160.
[24] P. Lu, T. Teranishi, K. Asakura, M. Miyake, N. Toshima, J. Phys. Chem. B 103 (1999) 9673–9682.
[25] P. Sangeetha, K. Shanthi, K.S.R. Rao, B. Viswanathan, P. Selvam, Appl. Catal. A 353 (2009) 160–165.
[26] F. Zhao, Y. Ikushima, M. Arai, J. Catal. 224 (2004) 479–483.
[27] L. Zhang, X. He, X. Xu, C. Liu, Y. Duan, L. Hou, Q. Zhou, C. Ma, X. Yang, R. Liu, F. Yang, L. Cui, C. Xu, Y. Li, Appl. Catal. B 203 (2017) 1–8.
[28] S. Samanta, S. Khilari, D. Pradhan, R. Srivastava, ACS Sustainable Chem. Eng. 5 (2017) 2562–2577.
[29] Z. Chen, S. Liu, M.Q. Yang, Y.J. Xu, ACS Appl. Mater. Interfaces 5 (2013) 4309–4319.
[30] X. Dai, M. Xie, S. Meng, X. Fu, S. Chen, Appl. Catal. B 158 (2014) 382–390.
[31] M.Q. Yang, B. Weng, Y.J. Xu, J. Mater. Chem. A 2 (2014) 1710–1720.
[32] M. Xie, X. Dai, S. Meng, X. Fu, S. Chen, Chem. Eng. J. 245 (2014) 107–116.
[33] L. Su, X. Ye, S. Meng, X. Fu, S. Chen, Appl. Surf. Sci. 384 (2016) 161–174.
[34] C. Ling, X. Ye, J. Zhang, J. Zhang, S. Zhang, S. Meng, X. Fu, S. Chen, Sci. Rep. 7 (2017) 27.
[35] M.Q. Yang, Y. Zhang, N. Zhang, Z.R. Tang, Y.J. Xu, Sci. Rep. 3 (2013) 3314.
[36] C. Huang, W. Ye, Q. Liu, X. Qiu, ACS Appl. Mater. Interfaces 6 (2014) 14469–14476.
[37] S. Meng, X. Ye, X. Ning, M. Xie, X. Fu, S. Chen, Appl. Catal. B 182 (2016) 356–368.
[38] M.Q. Yang, N. Zhang, M. Pagliaro, Y.J. Xu, Chem. Soc. Rev. 43 (2014) 8240–8254.
[39] X. Ning, S. Meng, X. Fu, X. Ye, S. Chen, Green Chem. 18 (2016) 3628–3639.
[40] X.H. Li, J.S. Chen, X. Wang, J. Sun, M. Antonietti, J. Am. Chem. Soc. 133 (2011) 8074–8077.
[41] X. Ke, X. Zhang, J. Zhao, S. Sarina, J. Barry, H. Zhu, Green Chem. 15 (2013) 236–244.
[42] B. Zhang, J. Li, B. Zhang, R. Chong, R. Li, B. Yuan, S.M. Lu, C. Li, J. Catal. 332 (2015) 95–100.
[43] M. Qamar, R.B. Elsayed, K.R. Alhooshani, M.I. Ahmed, D.W. Bahnemann, ACS Appl. Mater. Interfaces 7 (2015) 1257–1269.
[44] H.T. Ren, S.Y. Jia, J.J. Zou, S.H. Wu, X. Han, Appl. Catal. B 176–177 (2015) 53–61.
[45] C. Han, M.-Q. Yang, N. Zhang, Y.-J. Xu, J. Mater. Chem. A 2 (2014) 19156–19166.
[46] Y.P. Bhoi, B.G. Mishra, Chem. Eng. J. 316 (2017) 70–81.
[47] B.B. Kale, J.-O. Baeg, K.-j. Kong, S.-J. Moon, L.K. Nikam, K.R. Patil, J. Mater. Chem. 21 (2011) 2624–2631.
[48] Y.-P. Yuan, S.-W. Cao, L.-S. Yin, L. Xu, C. Xue, Int. J. Hydrogen Energy 38 (2013) 7218–7223.
[49] H. Liu, Z. Xu, Z. Zhang, D. Ao, Appl. Catal. B 192 (2016) 234–241.
[50] J. Hou, C. Yang, Z. Wang, S. Jiao, H. Zhu, RSC Adv. 2 (2012) 10330.
[51] O.V. Makarova, T. Rajh, M.C. Thurnauer, A. Martin, P.A. Kemme, D. Cropek, Environ. Sci. Technol. 34 (2000) 4797–4803.
[52] P. Roy, A.P. Periasamy, C.T. Liang, H.T. Chang, Environ. Sci. Technol. 47 (2013) 6688–6695.
[53] Z. Liu, Y. Huang, Q. Xiao, H. Zhu, Green Chem. 18 (2016) 817–825.
[54] A. Maldotti, L. Andreotti, A. Molinari, S. Tollari, A. Penoni, S. Cenini, J. Photochem. Photobiol. A 133 (2000) 129–133.
[55] R.A. Sanchez-Delgado, B.A. Oramas, J. Mol. Catal. 36 (1986) 283–291.
[56] T. Okano, K. Fujiwara, H. Konishi, J. Kiji, Chem. Lett. 10 (1981) 1083–1086.
[57] S. Füldner, P. Pohla, H. Bartling, S. Dankesreiter, R. Stadler, M. Gruber, A. Pfitzner, B. König, Green Chem. 13 (2011) 640–643.
[58] K. Imamura, T. Yoshikawa, K. Hashimoto, H. Kominami, Appl. Catal. B 134 (2013) 193–197.
[59] H. Miao, H. Li, Y. Cui, D. Tao, G. Wang, Y. Zhou, Mater. Lett. 133 (2014) 281–284.
[60] Q. Li, B. Guo, J. Yu, J. Ran, B. Zhang, H. Yan, J.R. Gong, J. Am. Chem. Soc. 133 (2011) 10878–10884.
[61] S. Liu, Z. Chen, N. Zhang, Z.-R. Tang, Y.-J. Xu, J. Phys. Chem. C 117 (2013) 8251–8261.
[62] L. Zhu, W.-C. Oh, RSC Adv. 5 (2015) 90321–90334.
[63] D.S. Kong, Langmuir 24 (2008) 5324–5331.
[64] Z.R. Tang, X. Yin, Y. Zhang, Y.J. Xu, Inorg. Chem. 52 (2013) 11758–11766.
[65] X. Wang, K. Maeda, A. Thomas, K. Takanabe, G. Xin, J.M. Carlsson, K. Domen, M. Antonietti, Nat. Mater. 8 (2009) 76–80.
[66] A. Tanaka, K. Hashimoto, H. Kominami, J. Am. Chem. Soc. 134 (2012) 14526–14533.
[67] S. Kitano, A. Tanaka, K. Hashimoto, H. Kominami, Phys. Chem. Chem. Phys. 16 (2014) 12554–12559.
[68] F. Mahdavi, T.C. Bruton, Y. Li, J. Org. Chem. 58 (1993) 744–746.
[69] V. Brezova, A. Blazkova, I. Surina, B. Havlinova, J. Photochem. Photobiol. A 107 (1997) 233–237.
[70] V. Brezová, P. Tarábek, D. Dvoranová, A. Staško, S. Biskupič, J. Photochem, Photobiol. A Chem. 155 (2003) 179–198.